

TYC 3159-6-1: a runaway blue supergiant

V. V. Gvaramadze,^{1,2*} A. S. Miroshnichenko,³ N. Castro,⁴ N. Langer⁴
and S. V. Zharikov⁵

¹*Sternberg Astronomical Institute, Lomonosov Moscow State University, Universitetskij Pr. 13, Moscow 119992, Russia*

²*Isaac Newton Institute of Chile, Moscow Branch, Universitetskij Pr. 13, Moscow 119992, Russia*

³*Department of Physics and Astronomy, University of North Carolina at Greensboro, Greensboro, NC 27402-6170, USA*

⁴*Argelander-Institut für Astronomie der Universität Bonn, Auf dem Hügel 71, 53121, Bonn, Germany*

⁵*Instituto de Astronomía, Universidad Nacional Autónoma de México, Ensenada, Mexico*

Accepted 2013 October 24. Received 2013 October 24; in original form 2013 July 26

ABSTRACT

We report the results of optical spectroscopy of a candidate evolved massive star in the Cygnus X region, TYC 3159-6-1, revealed via detection of its curious circumstellar nebula in archival data of the *Spitzer Space Telescope*. We classify TYC 3159-6-1 as an O9.5–O9.7Ib star and derive its fundamental parameters by using the stellar atmosphere code FASTWIND. The He and CNO abundances in the photosphere of TYC 3159-6-1 are consistent with the solar abundances, suggesting that the star only recently evolved off the main sequence. Proper motion and radial velocity measurements for TYC 3159-6-1 show that it is a runaway star. We propose that Dolidze 7 is its parent cluster. We discuss the origin of the nebula around TYC 3159-6-1 and suggest that it might be produced in several successive episodes of enhanced mass-loss rate (outbursts) caused by rotation of the star near the critical, Ω -limit.

Key words: circumstellar matter – stars: emission-line, Be – stars: fundamental parameters – stars: individual: TYC 3159-6-1 – supergiants – open clusters and associations: individual: Dolidze 7

1 INTRODUCTION

A significant fraction of massive stars leave the confines of their parent clusters because of few-body dynamical encounters with other cluster’s members or binary-supernova explosions, and spread out into the Galactic disk and halo to form the population of field stars. Some of the field stars possess high space velocities (the so-called runaway stars; Blaauw 1961) and can reach large distances from their birthplaces. The runaway stars escape from the large-scale wind bubbles, created around their parent clusters by the cumulative effect of stellar winds and supernovae, and their individual wind bubbles transform into bow shocks (Weaver et al. 1977). Depending on the physical properties (temperature, number density) of the ambient interstellar medium (ISM), the bow shocks might be generated and observable during most of the lifetime of runaway stars (Huthoff & Kaper 2002). This makes them the most wide-spread sort of parsec-scale nebulae associated with the field OB stars (e.g. van Buren, Noriega-Crespo & Dgani 1995; Peri et al. 2012).

The infrared (IR) surveys carried out by the *Spitzer*

Space Telescope (Werner et al. 2004) and the *Wide-field Infrared Survey Explorer* (*WISE*; Wright et al. 2010) greatly increased the number of known bow shocks. Also very important is that they revealed numerous compact nebulae of various morphologies, which are reminiscent of circumstellar nebulae observed around evolved massive stars (Gvaramadze, Kniazev & Fabrika 2010; Wachter et al. 2010; Mizuno et al. 2010). Follow-up spectroscopy of central stars of these nebulae resulted in the discovery of a large number of massive stars at the blue supergiant, luminous blue variable (LBV) and Wolf-Rayet stages (e.g. Gvaramadze et al. 2012a and earlier papers; Wachter et al. 2010). The short duration of these transient phases in the life of massive stars (a factor of 10 to 100 shorter than the main-sequence phase) implies that their circumstellar nebulae are rare objects. On the other hand, the rich morphological diversity of these nebulae (from circular to bipolar and triple-ring shape) points to the existence of several mechanisms responsible for their production and shaping. The detection of new examples of circumstellar nebulae allow us to not only reveal evolved massive stars, but it might also be crucial for better understanding the origin of these nebulae and the post-main-sequence evolution of their central stars.

In this paper, we report the discovery of a blue su-

* E-mail: vgvaram@mx.iki.rssi.ru

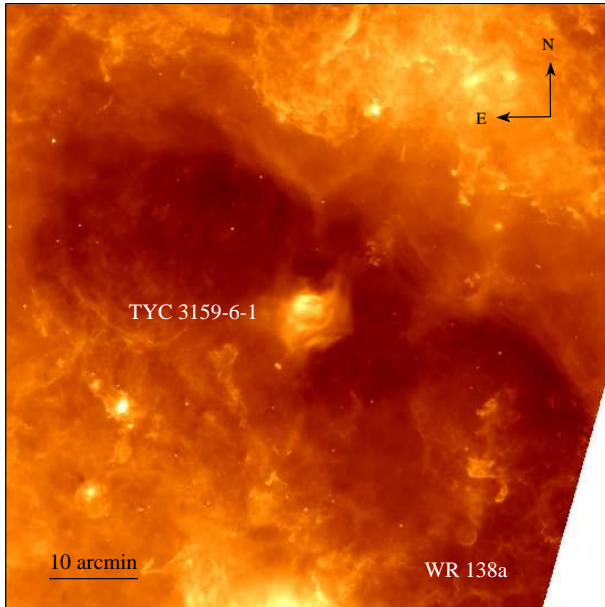


Figure 1. MIPS $24\ \mu\text{m}$ image of the field containing two IR nebulae associated with TYC 3159-6-1 (the subject of this paper) and the WN8-9h star WR 138a.

pergiant star in the Cygnus X region through detection of its associated nebula in the archival data of the *Spitzer Space Telescope* and follow-up optical spectroscopy. The star, TYC 3159-6-1, and the nebula are presented in Section 2. The spectral classification of TYC 3159-6-1 and the results of modelling of its spectrum with the stellar atmosphere code FASTWIND are given in Section 3. In Section 4, we show that TYC 3159-6-1 is a runaway star, whose likely birthplace is the star cluster Dolidze 7. The possible origin of the nebula around TYC 3159-6-1 is discussed in the same section.

2 TYC 3159-6-1 AND ITS ASSOCIATED MID-INFRARED NEBULA

The nebula around TYC 3159-6-1 was discovered during our search for evolved massive stars around the Cyg OB2 association via detection of their circumstellar nebulae (e.g. Gvaramadze et al. 2009, 2010). The search was carried out by using archival data originating from the Cygnus-X *Spitzer* Legacy Survey (Hora et al. 2008)¹. This survey covers 24 square degrees in Cygnus X, one of the most massive star-forming complexes in the Milky Way (e.g., Reipurth & Schneider 2008), and provides images at 24 and $70\ \mu\text{m}$ obtained with the Multiband Imaging Photometer for *Spitzer* (MIPS; Rieke et al. 2004) and at 3.6 , 4.5 , 5.8 , and $8.0\ \mu\text{m}$ obtained with the Infrared Array Camera (IRAC; Fazio et al. 2004). The resolution of the MIPS 24 and $70\ \mu\text{m}$ images is ≈ 6 and 18 arcsec, respectively, while that of the IRAC images is ≈ 1 arcsec.

Visual inspection of the $24\ \mu\text{m}$ survey data have led to the discovery of several compact nebulae. One of them turns out to be associated with the curious evolved massive star

MWC 349A (Gvaramadze & Menten 2012). Two other nebulae, MN114 and MN115² (Gvaramadze et al. 2010), are produced by the WN8-9h star WR 138a (Gvaramadze et al. 2009) and a candidate LBV star (Gvaramadze et al., in preparation), respectively. Another nebula, which is the subject of this paper, is associated with a moderately bright ($V \sim 11$ mag) star, located at only $\approx 0.5^\circ$ to the northeast of WR 138a and its ring nebula (see Fig.1 for the MIPS $24\ \mu\text{m}$ image of the field containing both nebulae). Subsequent examination of the SIMBAD data base³ revealed that this IR nebula was independently discovered by Takita et al. (2009) by using the 9 and $18\ \mu\text{m}$ images of the Cygnus X region taken as part of the *AKARI* mid-IR All-Sky Survey. These authors also identified a point-like source in the centre of the nebula with an optically visible star, listed in the Tycho catalog (Egret et al. 1992) as TYC 3159-6-1.

At $9\ \mu\text{m}$ the *AKARI* image shows an IR counterpart to TYC 3159-6-1 and a weak diffuse emission to the northeast of the star. At $18\ \mu\text{m}$ TYC 3159-6-1 is almost hidden in the bright emission of the nebula, which appears as a shell-like structure centred on TYC 3159-6-1 and two concentric, evenly spaced arc-like structures to the southwest of the star.

To determine the nature of TYC 3159-6-1, Takita et al. (2009) carried out follow-up optical spectroscopy of this star on 2007 September 21 using the 1.5-m telescope at the Gunma Astronomical Observatory. Although the obtained spectrum revealed the presence of the $H\alpha$ emission line, with an equivalent width (EW) of $-1.5\ \text{\AA}$, the spectral classification of the star was not carried out because of the low resolution ($R \sim 400 - 500$) of the spectroscopic material. Takita et al. (2009) considered three possibilities for the nature of TYC 3159-6-1: a nearby low-mass star, a highly reddened Be star, and an asymptotic giant branch star with a detached shell. They concluded, however, that none of them “can account for the observation consistently”. In Section 3.2, we show that TYC 3159-6-1 is an O9.5–O9.7 Ib star.

Using the observed $18\ \mu\text{m}$ flux of the nebula around TYC 3159-6-1, Takita et al. (2009) estimated the mass of the nebula to be $\sim 0.04 (d/1\text{kpc}) M_\odot$, where d is the distance to the star.

In Fig. 2 we present 24 , 12 and $8\ \mu\text{m}$ images of the field containing TYC 3159-6-1 and its circumstellar nebula, obtained with the MIPS, *WISE* and IRAC, respectively, and the Digitized Sky Survey II (DSS-II) red band (McLean et al. 2000) image of the same field. The MIPS $24\ \mu\text{m}$ image shows a bright, slightly asymmetric, incomplete shell of radius of ~ 1.4 arcmin, centred on a well-discerned point source – TYC 3159-6-1, and an arc-like structure with a radius of ≈ 2.5 arcmin to the southwest of the star. One can also see a more diffuse emission around the star (mostly concentrated to the southwest) of radius ~ 4 arcmin and two filaments extending for ~ 5 arcmin to the northwest. One of these filaments apparently crosses the bright shell and then curves to the northeast to form an incomplete circle of radius ~ 3 arcmin to the north of TYC 3159-6-1. This incomplete circle is also discernible in the *WISE* $12\ \mu\text{m}$ image and its

² In the SIMBAD database these nebulae are named [GKF2010] MN114 and [GKF2010] MN115.

³ <http://simbad.u-strasbg.fr/simbad/>

¹ <http://www.cfa.harvard.edu/cygnusX>

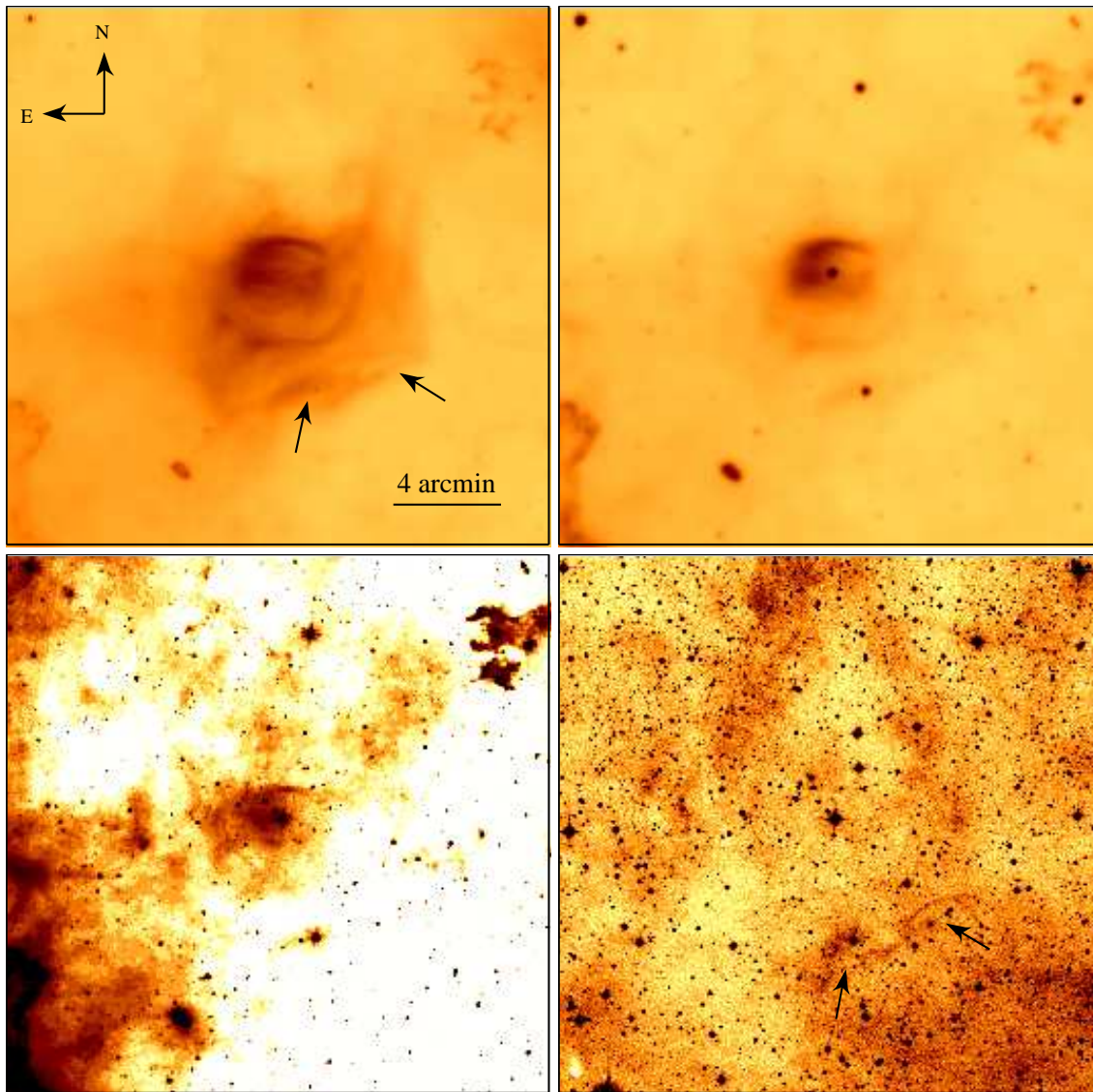


Figure 2. From left to right, and from top to bottom: MIPS $24\ \mu\text{m}$, *WISE* $12\ \mu\text{m}$, IRAC $8\ \mu\text{m}$, and DSS-II red band images of the field containing TYC 3159-6-1 and its circumstellar nebula. Arrows in the MIPS and DSS-II images point to filamentary structures visible both in the infrared and optical bands. The orientation and the scale of the images are the same. At a distance of 1.5 kpc, 1 arcmin corresponds to ≈ 0.43 pc.

Table 1. Details of TYC 3159-6-1.

Spectral type	O9.5–O9.7 Ib
RA(J2000)	$20^{\text{h}}18^{\text{m}}40^{\text{s}}.37$
Dec(J2000)	$41^{\circ}32'45''.0$
l	$78^{\circ}8320$
b	$3^{\circ}1505$
B (mag)	12.51 ± 0.28
V (mag)	10.88 ± 0.07
I (mag)	8.52 ± 0.06
J (mag)	6.82 ± 0.02
H (mag)	6.32 ± 0.04
K_s (mag)	5.95 ± 0.02
[3.4] (mag)	5.78 ± 0.05
[4.6] (mag)	5.47 ± 0.03
[12] (mag)	5.33 ± 0.02
[22] (mag)	3.41 ± 0.12

east boundary is clearly visible in the IRAC $8\ \mu\text{m}$ image. Moreover, the DSS-II image shows that the circle is flanked from the east and west sides by diffuse optical emission. The DSS-II image also shows distinct optical counterparts to filamentary structures at the southwest edge of the $24\ \mu\text{m}$ nebula (indicated by arrows in both images).

The details of TYC 3159-6-1 are summarized in Table 1. The coordinates and the B and V magnitudes are from the Tycho-2 Catalogue (Høg et al. 2000). The J , H and K_s magnitudes are taken from the 2MASS (Two Micron All Sky Survey) All-Sky Catalog of Point Sources (Cutri et al. 2003). For the sake of completeness we also give the I magnitude from the Amateur Sky Survey (TASS; Droege et al. 2006) and the *WISE* 3.4, 4.6, 12 and $22\ \mu\text{m}$ magnitudes from the *WISE* Preliminary Release Source Catalog (Cutri et al. 2012).

3 TYC 3159-6-1: A BLUE SUPERGIANT

To determine the spectral type of TYC 3159-6-1 and thereby to estimate the distance to this star, we observed TYC 3159-6-1 within the framework of our programme of spectroscopic follow-up of candidate massive stars revealed via detection of their circumstellar shells and bow shocks (e.g. Gvaramadze et al. 2011, 2012a, 2013; Stringfellow et al. 2012).

3.1 Spectroscopic observations and data reduction

We obtained two spectra of TYC 3159-6-1.

The first one was taken on 2012 November 14 with the 2.1-m telescope of the observatory of San Pedro Martir (Baja California, Mexico) using the REOSC Espresso échelle spectrograph (Levine & Chakrabarty 1995). This instrument gives a resolution of $0.12 \text{ \AA pixel}^{-1}$ near $H\alpha$ (that corresponds to a spectral resolving power of ~ 20000) using a UCL camera and a CCD-E2V chip of 2048×2048 pixels with a 13.5 micron pixel size. The spectra cover 28 orders and span the spectral range 3720–7200 \AA . One 20-minute exposure resulted in a range of signal-to-noise ratios (SNRs) from ~ 20 near $H\delta$ to ~ 80 near $H\alpha$.

The second spectrum was obtained on 2012 December 28 with the 2.7-m Harlan J. Smith telescope of the McDonald Observatory using a coudé échelle spectrograph (Tull et al. 1995) that provides a spectral resolving power of 60000 in the range 3600–10500 \AA . One 15-minute exposure resulted in a range of SNRs from ~ 15 near $H\delta$ to over 100 redward of $H\alpha$.

Both spectra were reduced using the IRAF⁴ software and re-binned for improving the SNR without affecting the spectral resolution. EWs, FWHMs and heliocentric radial velocities (RVs) of main lines in the spectrum of TYC 3159-6-1 are summarized in Table 2. The accuracies of EW, FWHM and RV measurements are $\pm(0.02\text{--}0.03) \text{ \AA}$, $\pm 0.1 \text{ \AA}$ and $\pm 1 \text{ km s}^{-1}$, respectively. Using the He I lines, we derived the heliocentric radial velocity of TYC 3159-6-1 of $v_{r,\text{hel}} = -35.8 \pm 3.0 \text{ km s}^{-1}$.

3.2 Spectral classification of TYC 3159-6-1

Fig. 3 presents the normalized spectrum of TYC 3159-6-1 taken on 2012 November 14. The spectrum is dominated by absorption lines of H I and He I. $H\alpha$ is in emission and shows a P Cygni profile. The He II $\lambda\lambda 4200, 4542, 4686$ and 5411 absorption lines are weak, which implies that TYC 3159-6-1 is of spectral type earlier than B1 (Walborn & Fitzpatrick 1990). The Mg II $\lambda 4481$ line is weak, which is typical of late O-B0 stars. The Si IV $\lambda\lambda 4089, 4116$, Si III $\lambda 4552$, N III $\lambda 4097$, and the blend of the C III $\lambda\lambda 4647, 4650, 4651$ and O III $\lambda 4650$ lines are clearly visible. The high interstellar extinction towards the star (≈ 6 mag; see Section 3.4) is manifested in numerous diffuse interstellar bands (DIBs), of which the most prominent are at 4429, 4727, 4762, 5780, 5797, 5850 and 6614 \AA .

⁴ IRAF: the Image Reduction and Analysis Facility is distributed by the National Optical Astronomy Observatory (NOAO), which is operated by the Association of Universities for Research in Astronomy, Inc. (AURA) under cooperative agreement with the National Science Foundation (NSF).

Table 2. Equivalent widths (EWs), FWHMs and radial heliocentric velocities (RVs) of main lines in the spectrum of TYC 3159-6-1 taken on 2012 November 14. The negative value of EW of the $H\alpha$ line corresponds to its emission component. For the sake of comparison, we also provide EWs (in brackets) of the components of the $H\alpha$ line from the spectrum taken on 2012 December 28.

$\lambda_0(\text{\AA})$ Ion	EW(λ) (\AA)	FWHM(λ) (\AA)	RV (km s^{-1})
4471 He I	0.73	2.60	-38.7
4713 He I	0.37	2.40	-36.7
4861 H β	1.48	5.23	-60.6
4922 He I	0.63	3.04	-30.7
5876 He I	1.43	4.32	-36.9
6563 H α	0.09 (0.49)		-220.3
6563 H α	-0.86 (-0.26)		-7.7
6678 He I	0.81	3.95	-36.1

The higher resolution of the spectrum taken on 2012 December 28 allowed us to resolve the Na I $\lambda\lambda 5890, 5896$ absorption lines into three components with $RV \approx -38, -22$ and -4 km s^{-1} (see Fig. 4). Two saturated components of these lines are of interstellar origin. RV of the third (most blueshifted) component of -38 km s^{-1} is close to $v_{r,\text{hel}}$, which suggests that this absorption originates in the circumstellar material.

The relative strength of the He II $\lambda 4542$ line with respect to the He I $\lambda 4388$ and Si III $\lambda 4552$ ones implies that TYC 3159-6-1 is of O9.5–O9.7 spectral type, while that of the lines He II $\lambda 4686$ and He I $\lambda 4713$ indicates luminosity class Ib (Sota et al. 2011). This spectral classification is consistent with the non-detection of the Si III $\lambda 5740$ line, which is observed in the spectra of supergiants of spectral types B0 and later (Miroshnichenko et al. 2004), but absent in those of O9–O9.5 ones.

Comparison of the two spectra revealed significant variability in the $H\alpha$ line profile and the strength of its emission and absorption components (see Fig. 5 and Table 2). Moreover, the emission component in both spectra became much weaker than that in the spectrum taken five years earlier by Takita et al. (2009). Such changes in the $H\alpha$ line (caused by the variability of the stellar wind) are typical of O supergiants (e.g. Markova et al. 2005).

3.3 Spectral analysis and stellar parameters

To derive the fundamental parameters of TYC 3159-6-1, we modelled its spectrum (taken on 2012 November 14) using the stellar atmosphere code FASTWIND (Fast Analysis of STellar atmospheres with WINDs; Santolaya-Rey, Puls & Herrero 1997; Puls et al. 2005). The code takes into account non-local thermodynamical equilibrium effects in spherical symmetry with an explicit treatment of the stellar wind effects by considering a β -like wind velocity law (Schaerer & Schmutz 1994). FASTWIND generates realistic models in a short period of time when compared with other similar codes, which is crucial for building large sets of models.

Characterization of optical spectra of late O- and early B-type stars can be established on well known lines between $\sim 4000 - 7000 \text{ \AA}$ (e.g. Crowther, Lennon & Walborn 2006). For instance, the determination of temperature and surface

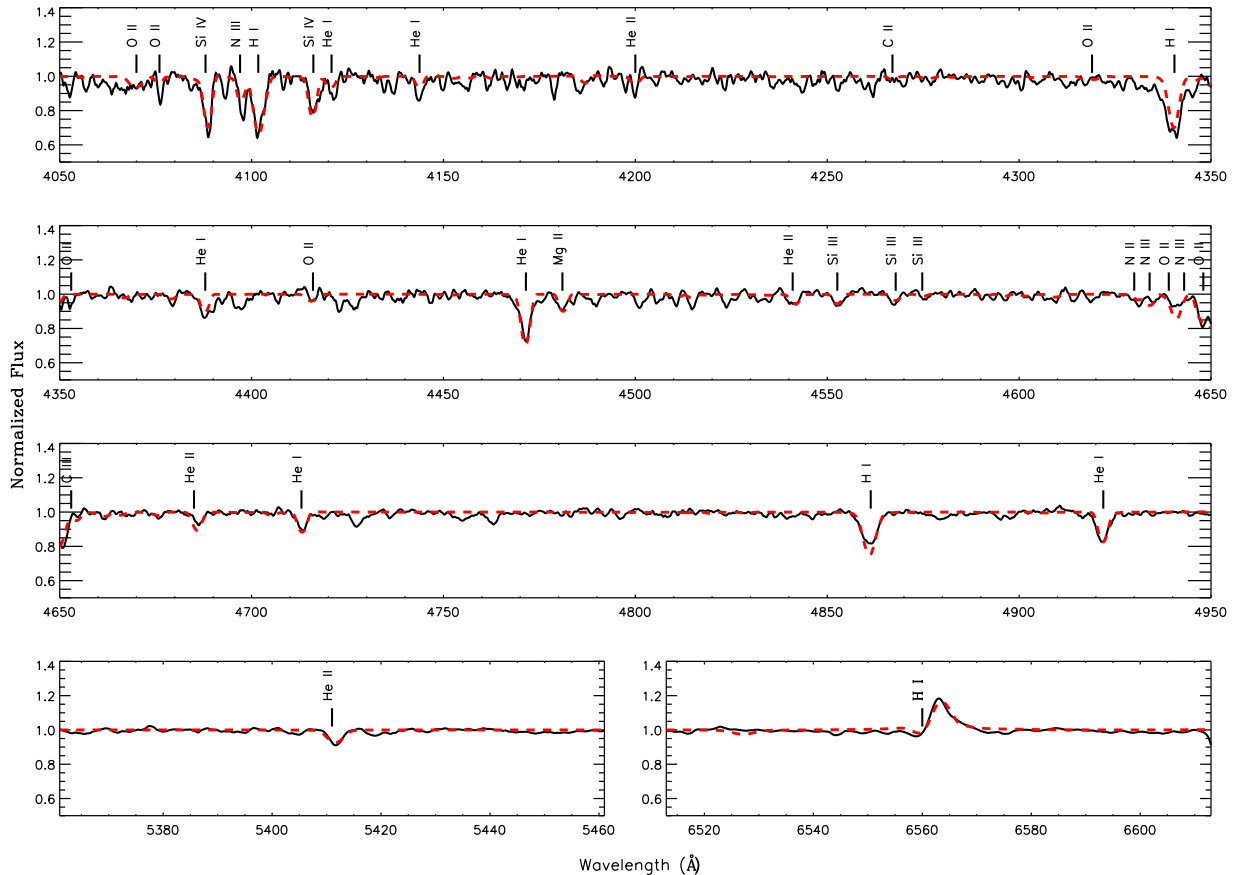


Figure 3. Normalized and re-binned spectrum of TYC 3159-6-1 taken on 2012 November 14, compared with the best-fitting FASTWIND model (red dashed line) with the parameters as given in Table 3. The lines fitted by the model are highlighted.

gravity can be achieved through the simultaneous fit of the ionization balance of different ionization stages of the same element (e.g. Si IV/Si III), and the fit to Balmer line wings. Nonetheless, the low SNR of the available spectroscopic material makes this procedure challenging. To tackle this issue, the technique suggested by Urbaneja et al. (2005) for low SNR spectral analysis was employed. We selected the main lines observed in TYC 3159-6-1, i.e. H I, He I–II and Si III–IV, and looked for the combination of stellar parameters which best reproduce the spectrum. This analysis was based on a large grid of FASTWIND stellar atmosphere models and a package of routines designed for automatic and fast search for best possible matches through a χ^2 minimization (see Lefever 2007). Afterwards, a set of tailored models was computed by varying the abundances of the CNO elements in steps of 0.20 dex. A complete description of the technique and the stellar parameters covered by the grid of stellar models can be found in Castro et al. (2012).

Each FASTWIND model is defined by nine parameters: effective temperature, T_{eff} , surface gravity, g , radius, R_* , helium abundance, He/H, microturbulence, ξ , metallicity, Z , wind velocity law, β , wind terminal velocity, v_∞ , and mass-loss rate, \dot{M} . Some of these parameters can be constrained using empirical calibrations. The stellar radius was estimated for the given pair ($T_{\text{eff}}, \log g$) through the

flux-weighted gravity–luminosity relationship (Kudritzki, Bresolin & Przybilla 2003):

$$M_{\text{bol}} = (3.41 \pm 0.16)(\log g_{\text{F}} - 1.5) - (8.02 \pm 0.04), \quad (1)$$

where M_{bol} is the bolometric magnitude and $\log g_{\text{F}} = \log g - 4 \log(T_{\text{eff}} \times 10^{-4})$. Since v_∞ cannot be constrained from the optical spectrum alone (Puls, Vink & Najarro 2008), we derived it from the escape velocity by using an empirical calibration [see equation (2) in Castro et al. 2012]. Moreover, Puls et al. (1996) showed that different combinations of \dot{M} , R_* and v_∞ can produce the same emergent line profiles as long as the optical depth invariant,

$$Q = \frac{\dot{M}}{(R_* v_\infty)^{3/2}}, \quad (2)$$

remains constant (here \dot{M} , R_* and v_∞ are in units of M_\odot , R_\odot and km s^{-1} , respectively). Since R_* and v_∞ are not free parameters, variations of \dot{M} are equivalent to variations of Q .

The low SNR prevents us from exploring the possible effect of macroturbulence on broadening of line shapes (Ryans et al. 2002; Hunter et al. 2008). Assuming that the broadening is due only to rotation, we derive a projected rotational velocity of 115 km s^{-1} . A similar estimate can be obtained from the relationship between the FWHM of the He I $\lambda 4471$ line and the projected rotational velocity,

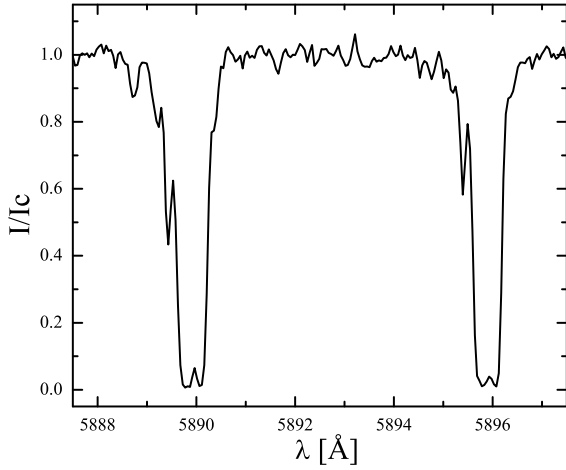


Figure 4. Na I D-lines in the higher-resolution spectrum of TYC 3159-6-1 taken on 2012 December 28. Two saturated components of the lines are of interstellar origin, while the third (most blueshifted) one may be formed in the circumstellar environment. The intensity is normalized to the local continuum, the wavelength scale is heliocentric.

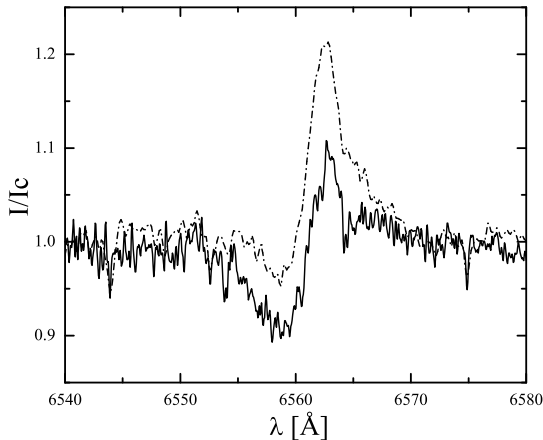


Figure 5. $H\alpha$ line profiles in the spectra of TYC 3159-6-1. The dash-dotted line shows the profile from 2012 November 14, while the solid line shows the one from 2012 December 28. Weak lines inside and around $H\alpha$ are telluric. The intensity and wavelength are in the same units as in Fig. 4.

$v \sin i = 41.25 \text{ FWHM}(4471) \text{ km s}^{-1}$ (Steele, Negueruela & Clark 1999), which for $\text{FWHM}(4471)=2.60 \text{ \AA}$ (see Table 2) and after correction for the instrumental FWHM of 0.3 \AA gives $v \sin i \approx 107 \text{ km s}^{-1}$. These estimates should be considered as an upper limit to the projected stellar rotational velocity because the macroturbulence could significantly contribute to the line broadening.

The best-fitting model for TYC 3159-6-1 is overlaid

Table 3. Stellar parameters for TYC 3159-6-1.

T_{eff} (kK)	27.0 ± 2.1
$\log g$ (cgs)	2.8 ± 0.2
R_* (R_{\odot}) (adopted)	32
He/H (by number)	0.10 ± 0.02
ξ (km s^{-1})	32 ± 13
v_{∞} (km s^{-1}) (adopted)	1200
β	2.2
$v \sin i$ (km s^{-1})	115
$\log Q$	-12.7 ± 0.2

Table 4. CNO elemental abundances (by number) in TYC 3159-6-1. The solar abundances are from Asplund et al. (2009).

$\log(X/H) + 12$	TYC 3159-6-1	Sun
C	$8.0^{+0.5}_{-0.3}$	8.43
N	$7.6^{+0.2}_{-0.4}$ ($8.0^{+0.2}_{-0.4}$) ^a	7.83
O	$8.5^{+0.4}_{-0.6}$	8.69

^a Based only on the N III $\lambda 4097$ line. See text for details.

on the observed (normalized) spectrum in Fig. 3, while the stellar parameters derived from this model are compiled in Table 3 and show a good agreement with those typical of O9.5I–B0I stars (e.g. Crowther et al. 2006). The errors quoted in the table were set at 95 per cent of probability distributions obtained during the quantitative analysis of the spectrum.

Constraining chemical abundances in low SNR data is also a challenging process. Nonetheless, the automatic routines were designed for gaining as much as possible the information hidden in the spectrum. Table 4 gives the CNO chemical abundances with the errors established at 95 per cent of the probability distribution found for each element. All three abundances are consistent within the margins of error with the solar ones (Asplund et al. 2009). The carbon abundance taken at face value shows depletion with respect to the solar one, which is expected for an atmosphere mixed with processed material from inner layers (see Langer 2012 and references therein). For nitrogen we derived two abundances. The first one is based on the simultaneous fit of all the nitrogen lines detected in the spectrum and the second one (given in Table 4 in brackets) was derived by fitting only the N III $\lambda 4097$ line (cf. Crowther et al. 2006). Both abundances agree within errors with the solar one, but the second one might also indicate a moderate enhancement of the nitrogen. We expect that the discrepancy in the nitrogen abundance estimates will be resolved with the next generation of FASTWIND nitrogen atomic models (Rivero González, Puls & Najarro 2011). The oxygen abundance was set by several very weak lines, which are blurred by the noise (see Fig. 3), so that it should be considered as an upper limit.

3.4 Reddening and distance to TYC 3159-6-1

To estimate the distance to TYC 3159-6-1, one can use the observed photometry of this star and the synthetic *UBVJHK* photometry of Galactic O stars by Martins & Plez (2006), which for an O9.5I star gives the *V*- and *K*-band absolute magnitudes, M_V and M_K , and the intrinsic

Table 5. Estimates of the colour excess, $E(B - V)$, towards TYC 3159-6-1 based on the EWs of DIBs at $\lambda 5780$, $\lambda 5797$ and $\lambda 8620$.

DIB (Å)	EW(λ) (Å)	$E(B - V)$ (mag)
5780	0.68 ± 0.03	1.34 ± 0.10
5797	0.26 ± 0.03	1.73 ± 0.10
8620	0.43 ± 0.03	1.16 ± 0.09

colours $(B - V)_0$ and $(J - K)_0$ of -6.34 , -5.52 , -0.26 and -0.21 mag, respectively. Using these figures and the B , V , J and K_s magnitudes from Table 1, one can estimate the V - and K -band extinction towards TYC 3159-6-1 and the distance modulus of this star with help of the relationships:

$$A_V = 3.1[(B - V) - (B - V)_0], \quad (3)$$

$$A_K = 0.66[(J - K) - (J - K)_0], \quad (4)$$

$$DM_V = V - M_V - A_V, \quad (5)$$

$$DM_K = K - M_K - A_K, \quad (6)$$

where the standard total-to-selective absorption ratio $R = A_V/E(B - V) = 3.1$ is assumed, and $K = K_s + 0.04$ mag (Carpenter 2001). From equations (3)-(6), it follows that $A_V = 5.86 \pm 0.89$ mag, $A_K = 0.69 \pm 0.02$ mag, $DM_V = 11.36 \pm 0.89$ mag and $DM_K = 10.82 \pm 0.02$ mag. For the error calculation, only the errors of the photometry were considered. The derived distance moduli correspond to distances of $1.87^{+0.95}_{-0.63}$ kpc and 1.46 ± 0.12 kpc, respectively.

Although the above two distance estimates are consistent with each other within the margins of error, we note that the distance based on the optical photometry might be overestimated because of anomalous reddening towards the star (e.g. caused by destruction of dust particles responsible for the visible extinction by stellar winds, interstellar shocks and/or radiation field). From equations (5) and (6) it follows that DM_V and DM_K can be reconciled with each other if $R \approx 3.4$. In this connection, we note that $R = 3.4 \pm 0.1$ was derived towards the cluster NGC 6910 (located at ≈ 1 degree to the southeast of TYC 3159-6-1; see Fig. 6) on the basis of photoelectric $UBVR$ photometry for 132 cluster members (Shevchenko, Ibragimov & Chernysheva 1991). In what follows, we adopt the distance based on the 2MASS photometry, i.e. $d \approx 1.5$ kpc (see also Section 4.2). At this distance, 1 arcmin corresponds to ≈ 0.43 pc.

The distance to TYC 3159-6-1 can also be estimated using EWs of the Na I D-lines. According to Beals & Oke (1953), $d = 1.6D$ kpc, where D is the average EW of the D_1 and D_2 lines in Å. With $EW(D_1) = 0.81$ Å and $EW(D_2) = 0.71$ Å, measured in the higher resolution (McDonald) spectrum, one obtains $d \approx 1.2$ kpc. This distance estimate is supported by a finding by Hobbs (1974) that the EW of the D_2 line grows on average at 0.60 Å/kpc, which implies $d \approx 1.2$ kpc as well (cf. van Kerkwijk, van Oijen & van den Heuvel 1989). The estimates based on the sodium lines should be considered as lower limits because both lines in the spectrum of TYC 3159-6-1 are saturated.

Alternatively, the extinction (and distance) towards TYC 3159-6-1 can be derived using the correlation between

the intensity of the DIBs and the colour excess $E(B - V)$ (see Herbig 1995 for a review). In Table 5 we provide estimates of $E(B - V)$ based on EWs of DIBs at $\lambda 5780$, $\lambda 5797$ and $\lambda 8620$ ⁵, and the relationships given in Herbig (1993) and Munari et al. (2008). Using these estimates and assuming $R = 3.4$, from equation (5) one can obtain a distance towards TYC 3159-6-1 of ≈ 3.4 , 1.9 and 4.5 kpc, respectively. The discrepancy between these distance estimates and that based on the 2MASS photometry could be due to a patchy distribution of the obscuring material (and the carriers of the DIBs) in the direction of Cygnus X (Schneider et al. 2006).

3.5 Luminosity and evolutionary status of TYC 3159-6-1

Using equation (1) and $\log g$ and T_{eff} from Table 3, one finds the bolometric magnitude of TYC 3159-6-1 of $M_{\text{bol}} = -9.47 \pm 0.83$ mag, which translates into the bolometric luminosity of $\log(L/L_{\odot}) = 0.4(4.74 - M_{\text{bol}}) = 5.68 \pm 0.33$. This luminosity implies that the zero-age main-sequence (ZAMS) mass of TYC 3159-6-1 was of $40 \pm 15 M_{\odot}$ (e.g. Ekström et al. 2012). Then using R_* and $\log g$, one can derive the current mass of TYC 3159-6-1 of $M_* \approx 23_{-9}^{+14} M_{\odot}$ (the quoted errors are based only on the errors of the gravity and did not take into account the possible range of R_* implied by uncertainties in the luminosity and temperature). Taken at face value, this mass implies that TYC 3159-6-1 has already lost about a half of its initial mass and now experiences a blue loop after the brief red supergiant phase of evolution (e.g. Ekström et al. 2012). This possibility however is inconsistent with the He and CNO abundances derived for TYC 3159-6-1, which rather suggest that the star only recently evolved off the main sequence and therefore preserved most of its ZAMS mass.

To further constrain M_* and thereby to estimate the age of TYC 3159-6-1, we compare its He and CNO abundances (see Tables 3 and 4 in Section 3.3) with those predicted by stellar evolutionary models (e.g., Brott et al. 2011; Ekström et al. 2012). Using the grid of models by Brott et al. (2011), we found that the main stellar parameters of TYC 3159-6-1 (temperature, luminosity, radius, gravity and abundances) can be matched very well with the $40 M_{\odot}$ model, provided that the age of the star is $\approx 4.0 - 4.5$ Myr. Particularly, a $40 M_{\odot}$ star with the initial rotation velocity of 161 km s^{-1} would have at the age of ≈ 4 Myr the following parameters: $T_{\text{eff}} \approx 25.7$ kK, $\log(L/L_{\odot}) \approx 5.62$, $R_* \approx 32.6 R_{\odot}$, $\log g \approx 2.97$, $v \sin i \approx 106 \text{ km s}^{-1}$. The CNO abundances of this star are 8.06, 7.88 and 8.53, respectively. All these parameters and abundances are in good agreement with those derived for TYC 3159-6-1 (see Tables 3 and 4). The Brott et al.'s models also suggest that the current mass of TYC 3159-6-1 should be $\approx 36 M_{\odot}$, which, considering the uncertainties on the stellar parameters, is consistent with the estimate of M_* given above. Thus, we conclude that TYC 3159-6-1 is a redward evolving star, which has only recently entered into the blue supergiant phase.

⁵ The latter DIB was detected in the McDonald spectrum of TYC 3159-6-1.

Table 6. Proper-motion, heliocentric radial velocity, peculiar transverse (in Galactic coordinates) and radial velocities, and the total space velocity of TYC 3159-6-1.

$\mu_\alpha \cos \delta$ (mas yr ⁻¹)	μ_δ (mas yr ⁻¹)	$v_{r,\text{hel}}$ (km s ⁻¹)	v_l (km s ⁻¹)	v_b (km s ⁻¹)	v_r (km s ⁻¹)	v_* (km s ⁻¹)
-2.4 ± 1.0	-0.1 ± 1.1	-35.8 ± 3.0	25.3 ± 7.4	20.1 ± 7.1	-25.8 ± 5.0	41.3 ± 6.5

4 DISCUSSION

4.1 TYC 3159-6-1 as a runaway

The enhanced brightness of the nebula along its northeast rim could be caused by motion of TYC 3159-6-1 in the northeast direction (cf. Danforth & Chu 2001; Gvaramadze et al. 2009). To check this possibility, we searched for proper motion measurements for TYC 3159-6-1 using the VizieR catalogue access tool⁶. We found several measurements of which the most recent one (and the one with the smallest claimed errors) is provided by the fourth U.S. Naval Observatory CCD Astrograph Catalog (UCAC4; Zacharias et al. 2013). This measurement is given in Table 6 along with the heliocentric radial velocity of the star (derived in Section 3.1), the components of its peculiar transverse velocity (in Galactic coordinates), v_l and v_b , the peculiar radial velocity, v_r , and the total peculiar (space) velocity, v_* . To derive the peculiar velocities, we used the Galactic constants $R_0 = 8.0$ kpc and $\Theta_0 = 240$ km s⁻¹ (Reid et al. 2009) and the solar peculiar motion $(U_\odot, V_\odot, W_\odot) = (11.1, 12.2, 7.3)$ km s⁻¹ (Schönrich, Binney & Dehnen 2010). For the error calculation, only the errors of the proper motion and the radial velocity measurements were considered.

The derived space velocity of ≈ 40 km s⁻¹ implies that TYC 3159-6-1 is a classical runaway star (Blaauw 1961; Cruz-González et al. 1974). From Table 6 it follows that TYC 3159-6-1 is moving in the northeast direction, i.e. towards the brightest arc of the IR nebula, with a transverse velocity of ≈ 32 km s⁻¹. Moreover, TYC 3159-6-1 is approaching us with a velocity of ≈ 25 km s⁻¹, so that the vector of its space velocity makes an angle of ≈ 50 degree with respect to our line-of-sight.

4.2 Parent cluster to TYC 3159-6-1

Fig. 6 shows the *Midcourse Space Experiment* (MSX) satellite (Price et al. 2001) $6^\circ \times 6^\circ$ image of the Cygnus X region. The position of TYC 3159-6-1 and the direction of its peculiar transverse velocity are indicated by a circle and an arrow, respectively. The solid line represents the trajectory of TYC 3159-6-1, as suggested by the proper motion measurements, while the dashed ones indicate 1 sigma uncertainties. Fig. 6 also shows positions of six star clusters, five of which are located within the error cone of the past trajectory of TYC 3159-6-1. The remaining one, NGC 6910, is located not far from the cone and potentially can be the parent cluster to TYC 3159-6-1, provided that its space velocity is pointed away from the cone. Let us discuss which of these six clusters might be the birthplace of TYC 3159-6-1.

In Table 7 we summarize distance and age estimates for

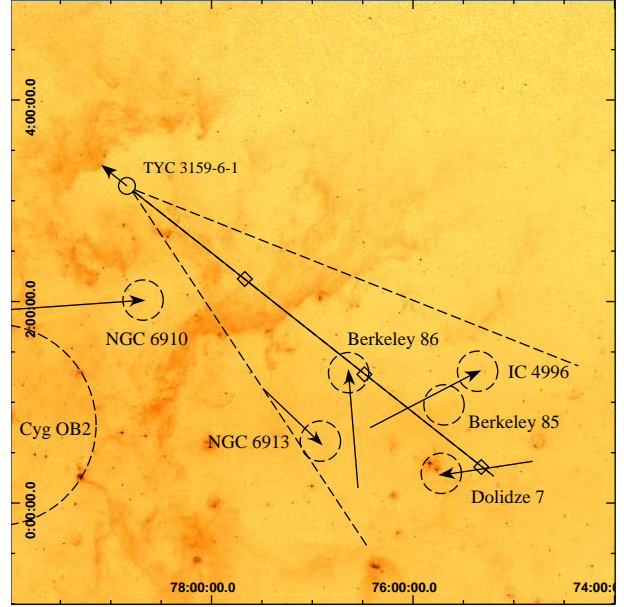


Figure 6. $6^\circ \times 6^\circ$ MSX $8.3 \mu\text{m}$ image of the Cygnus X region centred at $l = 77^\circ, b = 2^\circ$, with the position of TYC 3159-6-1 indicated by a circle. The arrow shows the direction of motion of TYC 3159-6-1, while a solid line indicates the trajectory of TYC 3159-6-1 (with 1 sigma uncertainties shown by dashed lines). The positions of the star 1, 2 and 3 Myr ago are marked by diamonds. The positions of six star clusters located near to or within the error cone of the past trajectory of TYC 3159-6-1 are indicated by small dashed circles. The arrows attached to these circles show the direction of clusters' peculiar motions, while their origins correspond to the positions of the clusters 4 Myr ago. The approximate boundary of the Cyg OB2 association is shown by a dashed circle of a diameter of 2 degree. The image is oriented with Galactic longitude (in units of degrees) increasing to the left and Galactic latitude increasing upwards. At a distance of 1.6 kpc, 1 degree corresponds to ≈ 27.5 pc. See text for details.

the six clusters (listed according to their right ascensions) as derived from literature. The very old age of Berkeley 85 allows us to exclude this cluster from further consideration. From the table it follows that the main problem with ascertaining the parent cluster to TYC 3159-6-1 is the uncertainty in distances to the clusters, which are based on spectrophotometric studies. This uncertainty is mainly caused by high and patchy extinction towards the Cygnus X region (e.g. Schneider et al. 2006) and by variations of reddening across the face of particular clusters (e.g. Turner & Forbes 1982; Wang & Hu 2000). On the other hand, there are strong indications that most molecular clouds in Cygnus X, and correspondingly their associated star clusters, form a coherent complex (Schneider et al. 2006; cf. Mel'nik & Efremov 1995), which is located at about the same distance as the

⁶ <http://vizier.u-strasbg.fr/cgi-bin/VizieR>

Table 8. Proper-motion measurements for star clusters located near to or within the error cone of the past trajectory of TYC 3159-6-1. For each measurement, the components of the peculiar transverse velocity (in Galactic coordinates) and the total space velocity, v_{tot} , are calculated and added to the table. See text for details.

Object	$\mu_\alpha \cos \delta$ (mas yr ⁻¹)	μ_δ (mas yr ⁻¹)	v_l (km s ⁻¹)	v_b (km s ⁻¹)	v_{tot} (km s ⁻¹)
IC 4996	-3.2 ± 0.1	-5.5 ± 0.1	-7.7 ± 0.8	4.0 ± 0.8	8.7 ± 0.8
Berkeley 86	-3.1 ± 0.3	-4.2 ± 0.2	0.7 ± 1.8	8.5 ± 2.1	8.5 ± 2.1
Dolidze 7	-1.6 ± 0.7	-4.2 ± 0.5	6.6 ± 4.1	-1.0 ± 4.6	6.7 ± 4.1
NGC 6910	-3.4 ± 0.3	-6.2 ± 0.3	-13.6 ± 1.9	1.2 ± 1.9	13.6 ± 1.9
NGC 6913	-1.5 ± 0.4	-4.7 ± 0.3	-4.2 ± 2.7	-4.0 ± 2.7	5.8 ± 2.7

Table 7. Distance and age estimates for star clusters located within or close to the error cone of the past trajectory of TYC 3159-6-1.

Object	d (kpc)	age (Myr)
IC 4996	1.6 ^{a,b} ; 1.7 ^c ; 2.0 ^d ; 2.3 ^e	6.3 ^c ; 9 ^a ; 10 ^b
Berkeley 85	1.6 ^d ; 1.8 ^b	1000 ^b
Berkeley 86	1.6 ^e ; 1.7 ^{f,d} ; 1.9 ^g	2–3 ^g ; 6 ^h ; 8.7 ^f
Dolidze 7	1.2 ⁱ ; 1.5 ^e ; 1.6 ^j ; 1.9 ^d	3 ^j ; 4 ^k ; 4–6 ^l
NGC 6910	1.6 ^m ; 1.8 ^d ; 2.3 ^e	6 ^m ; 6.5 ^e
NGC 6913	1.1 ⁿ ; 1.8 ^d ; 2.2 ^g	4–6 ^g

^aVancevicius et al. (1996); ^bMaciejewski & Niedzielski (2007); ^cKharchenko et al. (2005); ^dLe Duigou & Knödlseeder (2002); ^eBhavya et al. (2007); ^fDelgado, Alfaro & Cabrera-Cano (1997); ^gMassey, Johnson & Degioia-Eastwood (1995); ^hForbes (1981); ⁱTurner et al. (2006); ^jMassey, DeGioia-Eastwood & Waterhouse (2001); ^kPolcaro & Norci 1998; ^lOskinova et al. 2010; ^mKolaczkowski et al. (2004); ⁿWang & Hu (2000).

Cyg OB2 association (i.e. at $d \approx 1.4$ kpc; Rygl et al. 2012). The range of distances derived for the clusters in Table 7 allows the possibility that all of them might be the birthplace of TYC 3159-6-1. In the following we adopt a common distance of 1.6 kpc to all these clusters, where we took into account the fact that TYC 3159-6-1 is moving towards us with the velocity of ≈ 25 km s⁻¹ and therefore might travel ≈ 100 pc in the radial direction during its lifetime. We use this distance and the cluster proper motion measurements by Loktin & Bechenov (2003) to calculate the magnitude and direction of space velocities of the clusters and thereby to check whether their trajectories intersect in the past with that of TYC 3159-6-1 (cf. Schilbach & Röser 2008; Gvaramadze & Bomans 2008). The results of the calculations are summarized in Table 8. The derived space velocities of the clusters of ~ 10 km s⁻¹ are comparable to those of several star-forming regions around the Cyg OB2 association (Rygl et al. 2012). It is worth noting that these velocities do not show a regular pattern, which suggests the presence of large-scale turbulent motions in the parent molecular cloud of the clusters.

In Fig. 6 we show the trajectories of the clusters and their positions on the sky 4 Myr ago. One can see that NGC 6910 is moving in the “incorrect” direction, so that it cannot be the parent cluster to TYC 3159-6-1. The trajectories of the remaining four clusters are confined within

the error cone of the past trajectory of TYC3159-6-1 and therefore, in principle, they can intersect the trajectory of the star. Note however that the age estimates for IC 4996 (6–10 Myr) are inconsistent with the age of TYC 3159-6-1 of 4 Myr, which suggests that the cluster and the star are not related to each other. Moreover, although we cannot exclude the possibility that TYC 3159-6-1 was ejected from Berkeley 86 or NGC 6913, we note that these two clusters were at the periphery of the cone ~ 3 Myr ago, which makes Dolidze 7 the more likely candidate for the birthplace of the star. An indirect support to the physical relationship between TYC 3159-6-1 and Dolidze 7 comes from the presence in this cluster of the candidate LBV star V439 Cyg (Polcaro & Norci 1998; Polcaro, Norci & Miroshnichenko 2006), whose age and ZAMS mass of 4 Myr and 40 M_⊙, respectively (Polcaro & Norci 1998), are similar to those of TYC 3159-6-1.

It is also worth noting that the kinematic age of TYC 3159-6-1, i.e. the time elapsed since the ejection event, constitutes a significant fraction of its evolutionary one. This implies that the ejection of TYC 3159-6-1 into the field cannot be caused by a supernova explosion in a massive binary system (the companion star would simply have no time to end its life in a supernova), but is the result of dynamical three- or four-body encounter in the core of the parent cluster (cf. Gualandris, Portegies Zwart & Eggleton 2004; Gvaramadze et al. 2011).

4.3 Origin of the nebula around TYC 3159-6-1

The orientation of the peculiar transverse velocity of TYC 3159-6-1 and the arc-like appearance of the brightest part of the IR nebula (see the *WISE* 8 μm image in Fig. 2) suggest that the nebula might be a bow shock created because of interaction between the wind of the supersonically moving star and the ambient ISM. In this case, the radius of the arc would correspond to the stand-off distance of the bow shock, R_0 , which can be expressed through \dot{M} , v_∞ , v_* , and the number density of the local ISM, n_0 , as follows:

$$R_0 = \left(\frac{\dot{M} v_\infty}{4\pi \rho v_*^2} \right)^{1/2}, \quad (7)$$

where $\rho = \mu m_H n_0$, $\mu = 1.4$ is the mean molecular weight, and m_H is the mass of a hydrogen atom. For $R_0 \approx 0.46$ pc and $\dot{M} \approx 1.5 \times 10^{-6}$ M_⊙ yr⁻¹, derived from equation (2), one finds from equation (7) that $n_0 \approx 12$ cm⁻³, i.e. a quite reasonable figure (cf. Gvaramadze & Bomans 2008). The

bow shock interpretation for the nebula around TYC 3159-6-1, however, does not allow us to explain the complex appearance of the nebula as a whole, especially the northern curved filaments, which might be a signature of a bipolar outflow from the star. Instead, we suggest that the nebula is composed of material ejected by TYC 3159-6-1 in several successive episodes of enhanced wind mass loss or outbursts, similar to those observed in LBVs. Our suggestion is supported by the detection of the circumstellar component in the sodium doublet (Section 3.2), indicating the presence of significant amount of matter comoving with the star.

Several examples of bipolar nebulae are known to be associated with blue supergiants, of which the most spectacular are a triple-ring nebula produced by the progenitor star of the SN 1987A (Burrows et al. 1995) and hourglass-shaped nebulae around the Galactic blue supergiants Sher 25 (Brandner et al. 1997) and MN18 (Gvaramadze et al. 2010). Similar bipolar nebulae are also observed around candidate LBVs HD 168625 (Smith 2007) and MN13 (Gvaramadze et al. 2010; Wachter et al. 2011). The origin of these nebulae is still subject of debate, but there is consensus that different mechanisms might be responsible for their ejection and shaping (e.g. Morris 1981; García-Segura, Langer & Mac Low 1996; Chita et al. 2008).

Although all known (bipolar) circumstellar nebulae around massive stars are associated with stars evolved off the main sequence, it is still not clear at what post-main-sequence evolutionary phase they are ejected. According to most scenarios, this should happen when the star has already undergone a red supergiant phase, i.e. when the star is close to the endpoint of its life – the type II supernova explosion. Detection of the triple-ring nebula around the SN 1987A confirms that at least some circumstellar nebulae originate during the final phases of stellar evolution. On the other hand, analysis of chemical abundances in some nebulae associated with massive stars (including the nebula around Sher 25) argues against the possibility that these stars have evolved through the red supergiant phase, and suggests that they were ejected soon after the end of the main-sequence, i.e. at the beginning of the blue supergiant phase (Lamers et al. 2001; Hendry et al. 2008). The mildly enhanced He and N abundances derived for these nebulae can be understood if by the moment of ejection the stellar envelopes were enriched by processed material from the core because of rotationally induced mixing at or near the end of the main sequence. Accordingly, the central stars of these nebulae should be fast rotators for the mixing to occur.

As discussed in Section 3.5, the He and CNO abundances in the photosphere of TYC 3159-6-1 imply that the star only recently entered into the blue supergiant phase, which in turn implies that the nebula was ejected just after the main sequence. It is likely that the origin of this and other nebulae associated with (unevolved) blue supergiants is related to the fast rotation of their central stars (Lamers et al. 2001; Hendry et al. 2008). The post-main-sequence expansion of a fast-rotating star may result in the nearly critical rotation of its surface layers (Eriguchi et al. 1992), i.e. may bring the stellar envelope close to the Ω limit (Langer 1997, 1998; Maeder & Meynet 2000), which in turn may result in enhanced stationary or eruptive mass loss. Note that the moderate rotational velocity of TYC 3159-6-1 (see Section 3.3) does not contradict to the possibility that

this star was a fast rotator in the near past because its envelope might already lost a significant fraction of its angular momentum due to several episodes of mass ejection.

The morphology of the IR nebula associated with TYC 3159-6-1 suggests that it might be produced in three successive episodes of enhanced mass loss (outbursts) alternated with periods of quiescent mass loss. We speculate that the material ejected during the outbursts is concentrated near the equatorial plane of the fast-rotating star and that the ram pressure of the ISM due to the stellar motion makes this material lagging behind the star. Assuming that the ejected material expands with a velocity of $\sim 50 \text{ km s}^{-1}$ (which is typical of LBVs and related objects; Nota et al. 1995), one finds the dynamical age of the nebula of $\sim 3 \times 10^4$ yr. Moreover, from the almost equal separation between the southern edge of the nebula and the two concentric filaments within it one can derive that the duty cycle of the eruptive activity is of the order of $\sim 10^4$ yr. On the other hand, the presence of the curved filaments to the north of TYC 3159-6-1 suggests that the ejected material has a bipolar component as well. The polar outflows might originate simultaneously with the equatorial one (i.e. during the outburst) or because of collimation of the quiescent stellar wind by the dense material of the equatorial ejecta.

Assuming that the nebula is mainly composed of the material ejected during three successive outbursts of equal duration, τ , and that \dot{M} during these outbursts was $100\times$ the current mass-loss rate (e.g. Humphreys & Davidson 1994), one finds $\tau \sim 100$ yr, where we used the mass of the nebula of $\sim 0.06 M_{\odot}$ (see Section 2). Similarly, using the dynamical age of the nebula and the current \dot{M} of TYC 3159-6-1, one finds that the star has lost $\approx 0.05 M_{\odot}$ during the quiescent phases, which is comparable to the mass of the nebula. It is likely that the quiescent (high-velocity) wind escapes in the polar directions of the nebula and that it may be responsible for the origin of the curved filaments to the north of the nebula.

To conclude, we note that virtually in all scenarios for the origin of circumstellar nebulae around evolved massive stars it is assumed that these stars are static and therefore are surrounded by extended low-density wind bubbles formed during the main sequence. Correspondingly, it is assumed that the structure of these nebulae is not affected by density inhomogeneities in the ISM. In reality, however, the majority of known LBVs and related stars are located outside of any known star cluster and therefore most likely are runaways (Gvaramadze et al. 2012b). From this it follows that the field post-main-sequence massive stars are surrounded by the almost pristine ISM (whose structure is affected only by the stellar ionizing emission) and therefore their nebulae may directly interact with this (inhomogeneous) medium. The optical filaments to the south of TYC 3159-6-1 (see Fig. 2) might be a signature of such an interaction.

5 ACKNOWLEDGEMENTS

This work was partially supported by the DGAPA/PAPIIT project IN-103912. A.S.M. acknowledges financial support from the University of North Carolina at Greensboro and from its Department of Physics and Astronomy. We are

grateful to the referee for careful reading the manuscript and useful suggestions. This work has made use of the NASA/IPAC Infrared Science Archive, which is operated by the Jet Propulsion Laboratory, California Institute of Technology, under contract with the National Aeronautics and Space Administration, the SIMBAD database and the VizieR catalogue access tool, both operated at CDS, Strasbourg, France.

REFERENCES

- Asplund M., Grevesse N., Sauval A.J., Scott P., 2009, *ARA&A*, 47, 481
- Beals C.S., Oke J.B., 1953, *MNRAS*, 113, 530
- Bhavya B., Mathew B., Subramaniam A., 2007, *Bull. Astron. Soc. India*, 35, 383
- Blaauw A., 1961, *Bull. Astron. Inst. Netherlands*, 15, 265
- Brandner W., Grebel E.K., Chu Y.-H., Weis K., 1997, *ApJ*, 475, L45
- Brott I. et al., 2011, *A&A*, 530, A115
- Burrows C.J. et al., 1995, *ApJ*, 452, 680
- Carpenter J.M., 2001, *AJ*, 121, 2851
- Castro N. et al., 2012, *A&A*, 542, A79
- Chita S.M., Langer N., van Marle A.J., Garcia-Segura G., Heger A., 2008, *A&A*, 488, L37
- Crowther P.A., Lennon D.J., Walborn N.R., 2006, *A&A*, 446, 279
- Cruz-González C., Recillas-Cruz E., Costero R., Peimbert M., Torres-Peimbert S., 1974, *Rev. Mex. Astron. Astrofis.*, 1, 211
- Cutri R.M. et al., 2003, *VizieR Online Data Catalog*, 2246, 0
- Cutri R.M. et al., 2012, *VizieR Online Data Catalog*, 2311, 0
- Danforth C.W., Chu Y.-H., 2001, *ApJ*, 552, L155
- Delgado A.J., Alfaro E.J., Cabrera-Cano J., 1997, *AJ*, 113, 713
- Droege T.F., Richmond M.W., Sallman M.P., Creager R.P., 2006, *PASP*, 118, 1666
- Egret D., Didelon P., Mclean B.J., Russell J.L., Turon C., 1992, *A&A*, 258, 217
- Ekström S. et al., 2012, *A&A*, 537, A146
- Eriguchi Y., Yamaoka H., Nomoto K., Hashimoto M., 1992, *ApJ*, 392, 243
- Fazio G.G. et al., 2004, *ApJS*, 154, 10
- Forbes D., 1981, *PASP*, 93, 441
- García-Segura G., Langer N., Mac Low M.-M., 1996, *A&A*, 305, 229
- Gualandris A., Portegies Zwart S., Eggleton P.P., 2004, *MNRAS*, 350, 615
- Gvaramadze V.V., Bomans D.J., 2008, *A&A*, 490, 1071
- Gvaramadze V.V., Menten K.M., 2012, *A&A*, 541, A7
- Gvaramadze V.V., Kniazev A.Y., Fabrika S., 2010, *MNRAS*, 405, 1047
- Gvaramadze V.V., Kniazev A.Y., Chené A.-N., Schnurr O., 2013, *MNRAS*, 430, L20
- Gvaramadze V.V., Kniazev A.Y., Kroupa P., Oh S., 2011, *A&A*, 535, A29
- Gvaramadze V.V., Weidner C., Kroupa P., Pflamm-Altenburg J., 2012b, *MNRAS*, 424, 3037
- Gvaramadze V.V. et al., 2009, *MNRAS*, 400, 524
- Gvaramadze V.V. et al., 2012a, *MNRAS*, 421, 3325
- Hendry M.A., Smartt S.J., Skillman E.D., Evans C.J., Trundle C., Lennon D.J., Crowther P.A., Hunter I., 2008, *MNRAS*, 388, 1127
- Herbig G.H., 1995, *ARA&A* 33, 19
- Herbig G.H., 1993, *ApJ*, 407, 142
- Hobbs L.M., 1974, *ApJ*, 191, 381
- Høg E. et al., 2000, *A&A*, 355, L27
- Hora J.L. et al., 2008, *New Light on Young Stars: Spitzers View of Circumstellar Disks* (<http://www.ipac.caltech.edu/spitzer2008/proceedings.html>)
- Humphreys R.M., Davidson K., 1994, *PASP*, 106, 1025
- Hunter I., Lennon D.J., Dufton P.L., Trundle C., Simón-Díaz S., Smartt S.J., Ryans R.S.I., Evans C.J., 2008, *A&A*, 479, 541
- Huthoff F., Kaper L., 2002, *A&A*, 383, 999
- Kharchenko N.V., Piskunov A.E., Röser S., Schilbach E., Scholz R.-D., 2005, *A&A*, 438, 1163
- Kolaczowski Z., Pigulski A., Kopacki G., Michalska G., 2004, *Acta Astron.*, 54, 33
- Kudritzki R.P., Bresolin F., Przybilla N., 2003, *ApJ*, 582, L83
- Lamers H.J.G.L.M., Nota A., Panagia N., Smith L.J., Langer N., 2001, *ApJ*, 551, 764
- Langer N., 1997, in Nota A., Lamers H., eds, *ASP Conf. Ser. Vol. 120, Luminous Blue Variables: Massive Stars in Transition*. Astron. Soc. Pac., San Francisco, p. 83
- Langer N., 1998, *A&A* 329, 551
- Langer N., 2012, *ARA&A*, 50, 107
- Le Duigou J.M., Knödseder J., 2002, *A&A*, 392, 869
- Lefever K., 2007, PhD thesis, K. U. Leuven
- Levine S., Chakrabarty D., 1995, *IA-UNAM Technical Report MU-94-04*
- Loktin A.V., Beshenov G.V., 2003, *Astron. Rep.*, 47, 6
- Maciejewski G., Niedzielski A., 2007, *A&A*, 467, 1065
- Maeder A., Meynet G., 2000, *A&A*, 361, 159
- Markova N., Puls J., Scuderi S., Markov H., 2005, *A&A*, 440, 1133
- Martins F., Plez B., 2006, *A&A*, 457, 637
- Massey P., Johnson K.E., Degioia-Eastwood K., 1995, *ApJ*, 454, 151
- Massey P., DeGioia-Eastwood K., Waterhouse E., 2001, *AJ*, 121, 1050
- McLean B.J., Greene G.R., Lattanzi M.G., Pirenne B., 2000, in Manset N., Veillet C., Crabtree D., eds, *ASP Conf. Ser. Vol. 216, Astronomical Data Analysis Software and Systems IX*. Astron. Soc. Pac., San Francisco, p. 145
- Melnik A.M., Efremov Y.N., 1995, *Astron. Lett.*, 21, 10
- Miroshnichenko A.S. et al., 2004, *A&A*, 417, 731
- Mizuno D.R. et al., 2010, *AJ*, 139, 1542
- Morris M., 1981, *ApJ*, 249, 572
- Munari U. et al., 2008, *A&A*, 488, 969
- Nota A., Livio M., Clampin M., Schulte-Ladbeck R., 1995, *ApJ*, 448, 788
- Oskinova L.M., Gruendl R.A., Ignace R., Chu Y.-H., Hamann W.-R., Feldmeier A., 2010, *ApJ*, 712, 763
- Peri C.S., Benaglia P., Brookes D.P., Stevens I.R., Isequilla N.L., 2012, *A&A*, 538, A108
- Polcaro V.F., Norci L., 1998, *A&A*, 339, 75
- Polcaro V.F., Norci L., Miroshnichenko A.S., 2006, in Kraus M., Miroshnichenko A.S., eds, *Stars with the B[e] Phenomenon*. ASP Conf. Series, Vol. 355, p.197
- Price S.D., Egan M.P., Carey S.J., Mizuno D.R., Kuchar T.A., 2001, *AJ*, 121, 2819
- Puls J. et al., 1996, *A&A*, 305, 171
- Puls J., Vink J.S., Najarro F., 2008, *A&A Rev.*, 16, 209
- Puls J., Urbaneja M.A., Venero R., Repolust T., Springmann U., Jokuthy A., Mokiem M.R., 2005, *A&A*, 435, 669
- Reid M.J., Menten K.M., Zheng X.W., Brunthaler A., Xu Y., 2009, *ApJ*, 705, 1548
- Reipurth B., Schneider N., 2008, in *ASP Monograph Publications, Vol. 4, Handbook of Star Forming Regions, Vol. I: The Northern Sky*, ed. B.Reipurth (San Francisco: ASP), 36
- Rieke G.H. et al., 2004, *ApJS*, 154, 25
- Rivero González J.G., Puls J., Najarro F., 2011, *A&A*, 536, A58
- Ryans R.S.I., Dufton P.L., Rolleston W.R.J., Lennon D.J., Keenan F.P., Smoker J.V., Lambert D.L., 2002, *MNRAS*, 336, 577
- Rygl K.L.J. et al., 2012, *A&A*, 539, A79

- Santolaya-Rey A.E., Puls J., Herrero A., 1997, *A&A*, 323, 488
- Schaerer D., Schmutz W., 1994, *A&A*, 288, 231
- Schilbach E., Röser S., 2008, *A&A*, 489, 105
- Schneider N., Bontemps S., Simon R., Jakob H., Motte F., Miller M., Kramer C., Stutzki J., 2006, *A&A*, 458, 855
- Schönrich R., Binney J., Dehnen W., 2010, *MNRAS*, 403, 1829
- Shevchenko V.S., Ibragimov M.A., Chernysheva T.L., 1991, *SvA*, 35, 229
- Smith N., 2007, *AJ*, 133, 1034
- Sota A., Maíz-Apellániz J., Walborn N.R., Alfaro E.J., Barbá R.H., Morrell N.I., Gamen R.C., Arias J.I., 2011, *ApJS*, 139, 24
- Steele I.A., Negueruela I., Clark J.S., 1999, *A&AS*, 137, 147
- Stringfellow G.S., Gvaramadze V.V., Beletsky Y., Kniazev A.Y., 2012a, in Richards M.T., Hubeny I., eds, *Proc. IAU Symp.*, Vol. 282, p. 267
- Takita S. et al., 2009, *PASJ*, 61, 291
- Tull R.G., MacQueen P.J., Sneden C., Lambert D.L., 1995, *PASP*, 107, 251
- Turner D.G., Forbes D., 1982, *PASP*, 94, 789
- Turner D.G., Rohanizadegan M., Berdnikov L.N., Pastukhova E.N., 2006, *PASP*, 118, 1533
- Urbaneja M.A., Herrero A., Kudritzki R., Najarro F., Smartt S.J., Puls J., Lennon D.J., Corral L.J., 2005, *ApJ*, 635, 311
- van Buren D., Noriega-Crespo A., Dgani R., 1995, *AJ*, 110, 2914
- van Kerkwijk M.H., van Oijen J.G.J., van den Heuvel E.P.J., 1989, *A&A*, 209, 173
- Vansevičius V., Bridžius A., Pučinskas A., Sasaki T., 1996, *Baltic Astron.*, 5, 539
- Wachter S., Mauerhan J., van Dyk S., Hoard D. W., Morris P., 2011, *Bull. Soc. R. Sci. Liège*, 80, 291
- Wachter S., Mauerhan J.C., van Dyk S.D., Hoard D.W., Kafka S., Morris P.W., 2010, *AJ*, 139, 2330
- Walborn N.R., Fitzpatrick E.L., 1990, *PASP*, 102, 379
- Wang J.-J., Hu J.-Y., 2000, *A&A*, 356, 118
- Weaver R., McCray R., Castor J., Shapiro P., Moore R., 1977, *ApJ*, 218, 377
- Werner M.W. et al., 2004, *ApJS*, 154, 1
- Wright E.L. et al., 2010, *AJ*, 140, 1868
- Zacharias N., Finch C.T., Girard T.M., Henden A., Bartlett J.L., Monet D.G., Zacharias M.I., 2013, *AJ*, 145, 44